molecular pharmaceutics

Article

pubs.acs.org/molecularpharmaceutics

# Noninvasive Detection of Passively Targeted Poly(ethylene glycol) Nanocarriers in Tumors

Yashveer Singh,[†] Dayuan Gao,[†] Zichao Gu, Shike Li, Stanley Stein, and Patrick J. Sinko*

Department of Pharmaceutics, Ernest Mario School of Pharmacy, Rutgers, The State University of New Jersey, New Brunswick, New Jersey, United States

Supporting Information

**ABSTRACT:** The present studies noninvasively investigate the passive tumor distribution potential of a series of poly(ethylene glycol) (PEG) nanocarriers using a SkinSkan spectrofluorometer and an In Vivo Imaging System (IVIS) 100. Fluorescein conjugated PEG nanocarriers of varying molecular weights (10, 20, 30, 40, and 60 kDa) were prepared and characterized. The nanocarriers were administered intravenously to female balb/c mice bearing subcutaneous 4T1 tumors. Passive distribution was measured in vivo ($\lambda_{exc}$, 480 nm; $\lambda_{em}$, 515−520 nm) from the tumor and a contralateral skin site (i.e., control site). The signal intensity from the tumor was always significantly higher than that from the contralateral site. Trends in results between the two methods were consistent with tumor distribution increasing in a molecular weight-dependent manner (10 < 20 < 30 ≪ 40 ≪ 60 kDa). The 10 kDa nanocarrier was not detected in tumors at 24 h, whereas 40−60 kDa nanocarriers were detected in tumors for up to 96 h. The 30, 40, and 60 kDa nanocarriers showed 2.1, 5.3, and 4.1 times higher passive distribution in tumors at 24 h, respectively, as compared to the 20 kDa nanocarrier. The 60 kDa nanocarrier exhibited 1.5 times higher tumor distribution than 40 kDa nanocarrier at 96 h. Thus, PEG nanocarriers (40 and 60 kDa) with molecular weights close to or above the renal exclusion limit, which for globular proteins is ≥45 kDa, showed significantly higher tumor distribution than those below it. The hydrodynamic radii of PEG polymers, measured using dynamic light scattering (DLS), showed that nanocarriers obtained from polymers with hydrodynamic radii ≥8 nm exhibited higher tumor distribution. Ex vivo mass balance studies revealed that nanocarrier tissue distribution followed the rank order tumor > lung > spleen > liver > kidney > muscle > heart, thus validating the in vivo studies. The results of the current studies suggest that noninvasive dermal imaging of tumors provides a reliable and rapid method for the initial screening of nanocarrier tumor distribution pharmacokinetics.

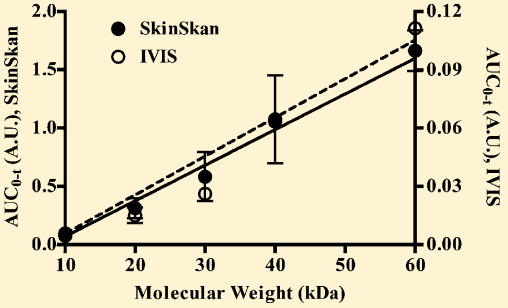


**KEYWORDS:** *enhanced permeability and retention (EPR), fluorescence, noninvasive detection, passive tumor distribution, PEG nanocarriers*

## INTRODUCTION

The field of polymer therapeutics has grown exponentially over last two decades, and several macromolecular drugs are now routinely used for various treatments.[1−4] The term polymer therapeutics encompasses polymer drugs,[5] polymer−protein conjugates,[1,2] polymer−drug conjugates,[1,2] polymeric assemblies with covalently attached drugs,[6] and polyplexes for gene delivery.[7]

Polymer−protein conjugates were the first in this class to be approved for clinical use.[1,2] Maeda and co-workers developed SMANCS in the early 1990s for treating hepatocellular carcinoma by conjugating neocarzinostatin (NCS, antitumor protein) to two polymer chains of styrene maleic anhydride (SMA).[8−10] PEG conjugates of enzymes like adenosine deaminase (Adagen)[11] and L-asparaginase (Oncaspar)[12] received FDA approval in 1990 and 1994 for treatment of severe combined immunodeficiency syndrome and acute lymphoblastic leukemia. Later, two PEG conjugates of interferon-$\alpha$ (IFN$\alpha$), Pegasys[13] and PEG-Intron,[14,15] were approved for treatment of hepatitis C. In 2010, PEGylated porcine-like uricase (Krystexxa, pegloticase) was approved for treatment of severe, treatment refractory chronic gout.[16] The advantages of using polymers for protein delivery are increased solubility, greater stability, prolonged plasma half-life, reduced immunogenicity, lower renal clearance, and decreased uptake by cells of reticuloendothelial system (RES).[1,2,17]

In 1975, Ringsdorf proposed the conceptual framework for using synthetic polymer conjugates for drug delivery.[18,19] Later, the Duncan[20] and Kopecek[21] groups together established the biological rationale for designing polymer−anticancer drug conjugates, and methods for their preclinical evaluation. They were the first to evaluate polymer−anticancer drug conjugates in a clinical trial. So far, none of the polymer−anticancer drug conjugates have been approved for human use, but several of them are undergoing clinical trials. Examples include *N*-(2-hydroxypropyl)-methacrylamide (HPMA)−doxorubicin (PK1),[22] HPMA−paclitaxel

**Received:** August 8, 2011
**Revised:** October 31, 2011
**Accepted:** November 12, 2011
**Published:** November 12, 2011

  

(PNU-166945),[23] HPMA−camptothecin (MAG-CPT),[24] PEG−camptothecin (prothecan),[25] polyglutamic acid (PGA)−paclitaxel (CT-2103, OPAXIO),[26] and PGA−camptothecin (CT-2106).[27] The rationale for designing polymer therapeutics for cancer treatment is that the attachment of a polymer to a drug limits cellular uptake by the endocytic route. This provides long circulating conjugates that achieve passive tumor distribution by EPR, as elucidated by Maeda and co-workers.[28,29]

EPR exploits the anatomical and physiological abnormalities of tumor tissue, particularly the tumor vasculature.[28−30] Angiogenesis is induced to meet the growing demand for nutrition and oxygen as the tumor grows and clusters together to reach the size of 2−3 mm. Neovasculature in tumor tissues is different from that in normal tissue, and is characterized by the presence of irregular, dilated, leaky or defective blood vessels; poorly aligned endothelial cells with large fenestrations; frequently absent or abnormal perivascular cells; and smooth muscle layers in vascular walls. In addition, the tumor vessels have wide lumens and impaired lymphatic drainage. These characteristic features work together to cause extensive leakage of the macromolecular component of blood plasma like polymers, lipidic particles, protein conjugates, liposomes, micelles, and nanoparticles into tumor tissues that, unlike small molecules, are unable to escape because of the slow venous return and poor lymphatic drainage from tumors. The EPR effect is influenced mainly by the molecular size and plasma residence time of polymers and nanoparticles. However, the neovasculature, tumor size, blood pressure, and vascular mediators like bradykinin, nitric oxide, prostaglandins, metalloproteinases, and peroxy nitrite are also known to influence tumor penetration and residence time.[30] Molecular size of the polymer, in turn, is primarily determined by the polymer molecular weight and also by their chemical nature, shape, and conformation in biological fluids. Similar passive accumulation approaches have been used by our group to target the liver and lungs, although the optimal size required for maximal targeting is much larger than for EPR-mediated accumulation in tumors.[31−33]

Advances in fundamental tissue optics and laser technology have led to the use of optical detection in diagnostics, which are advantageous because they employ nonionizing radiation, can be detected in minute amounts in tissues, and provide continuous data acquisition capabilities for real time monitoring.[34,35] Tissue spectroscopy has been used earlier to detect the distinguishing spectral features of malignant tissue in vitro and ex vivo,[36] endogenous[37,38]/exogenous[38] markers with sufficient sensitivity and specificity in malignant tissues, and to predict the outcome of cancer therapy. The skin is important for the development of noninvasive detection methods because of its accessibility. The endogenous fluorescence of the skin[39] and exogenous chromophores[40] have been previously used to noninvasively investigate nonmelanoma skin cancer, and oral premalignant and malignant lesions.

The aim of this work was to evaluate noninvasive dermal imaging techniques to reliably and rapidly screen nanocarrier tumor distribution pharmacokinetics. This was achieved by investigating the effect of PEG nanocarrier molecular weight on their EPR-mediated passive distribution in tumors using SkinSkan spectrofluorometer and the IVIS 100 system. PEG nanocarriers of varying molecular weights (10−60 kDa) were labeled with fluorescein using relatively stable thioether and amide bonds. The nanocarriers were intravenously administered to tumor-bearing mice, and in vivo fluorescence was measured from the tumor and a contralateral skin site. Both methods demonstrated that PEGs exhibit molecular weight-dependent passive distribution in tumors. Nanocarriers with molecular weight close to or above the renal exclusion limit (≥45 kDa for globular proteins) showed significantly higher tumor distribution than those with molecular weights well below the renal threshold. DLS studies with PEG polymers demonstrated that hydrodynamic radii of PEG increased with an increase in molecular weight, and were influenced by the molecular weight as well as polymer structure. The nanocarriers obtained from polymers with hydrodynamic radii of ≥8 nm exhibited higher tumor distribution due to the EPR effect. Higher passive distribution of PEG nanocarriers in tumors was further validated by ex vivo tissue distribution studies using a fluorescence plate reader.

## EXPERIMENTAL SECTION

**Materials.** The PEG-thiol ($M_w$ = 10, 20, and 30 kDa) and PEG-amine ($M_w$ = 40 and 60 kDa) polymers were obtained from NOF America (Whitefield, NY). The fluorescein-5-maleimide and fluorescein-5-succinimidyl ester were obtained from Anaspec (San Jose, CA). *N*,*N*-Dimethyl formamide (DMF) and ethylene diamine tetracetate (EDTA) were obtained from Sigma-Aldrich (St. Louis, MO), whereas Sephadex G50 (medium) was obtained from Thermo Fisher Scientific (Suwanee, GA). All cell culture reagents were obtained from Invitrogen (Carlsbad, CA), and Aerrane (isoflurane) was obtained from Baxter Healthcare Corporation (Deerfield, IL). The nanocarriers (2 mg/mL, water) were analyzed on a Waters Breeze gel-permeation chromatography (GPC) system equipped with refractive index and UV detectors, and a Waters Ultrahydrogel 1000 column (7.8 × 300 mm). Deionized (DI) water was used as mobile phase (flow rate: 1 mL/min). The molecular weights were estimated on a Voyager DE Pro matrix-assisted laser desorption ionization time-of-flight (MALDI-TOF) mass spectrometer from PerSeptive Biosystems in positive mode or 4700 Proteomics Analyzer MALDI-TOF/TOF system from Applied Biosystems (ABI). The hydrodynamic radii of polymers were measured by dynamic light scattering (DLS) on a Malvern Zetasizer Nano ZS. The polymer solutions were prepared in water (2 mg/mL) and passed through 0.2 μm membrane filters prior to analysis. The *in vivo* fluorescence spectra on mouse skin's surface were recorded using a Jobin Yuvon SkinSkan spectrofluorometer (Spex Industries, Edison, NJ), whereas the fluorescence from tissue homogenates was measured using a Genios microplate reader (Tecan, San Jose, CA). The noninvasive animal images were obtained on a Xenogen IVIS 100 imaging system from Caliper LifeSciences (Hopkinton, MA).

**Synthesis and Characterization of Fluorescein-Labeled PEG Nanocarriers.** *10, 20, and 30 kDa Nanocarriers.* The appropriate PEG-thiol (10, 20, or 30 kDa) polymer (50 mg) was taken in a round-bottom flask and dissolved in sodium phosphate buffer (0.1 M, pH = 7.4) containing EDTA (5 mM). Fluorescein-5-maleimide (5 equiv.) dissolved in DMF was added to the polymer solution. The reaction mixture was stirred in the dark at room temperature for 8 h. The product was purified on a Sephadex G 50 column using water as eluent. The reaction mixture was loaded onto the column, and high molecular weight fractions were eluted. The column was washed with water to remove the unreacted fluorescein. The high molecular weight fractions were pooled together and lyophilized to obtain pure nanocarriers as yellow flakes, which were characterized by GPC and MALDI-TOF.

*10 kDa.* Yield: 38 mg (73%). GPC: $t_R$ = 8.2 min (PEG-fluorescein) and 8.9 min (PEG-SH). MALDI-TOF ($m/z$):

calculated, 10291.37 Da; observed, 10393.7 Da (PEG-fluorescein).

*20 kDa.* Yield: 40 mg (78.4%). GPC: $t_R$ = 7.4 min (PEG-fluorescein) and 8.3 min (PEG-SH). MALDI-TOF ($m/z$): calculated. 20100 Da; observed. 21332 Da (PEG-fluorescein).

*30 kDa.* Yield: 40 mg (79.2%). GPC: $t_R$ = 6.3 min (PEG-fluorescein) and 7.9 min (PEG-SH). MALDI-TOF ($m/z$): calculated, 28873.37 Da; observed, 31659.34 Da (PEG-fluorescein).

*40 and 60 kDa Nanocarriers.* The appropriate PEG-amine (40 or 60 kDa) polymer (50 mg) was taken in a round-bottom flask and dissolved in sodium phosphate buffer (0.1 M, pH = 8.0). Fluorescein-5-succinimidyl ester (5 equiv) was added to the polymer solution, and the reaction mixture was stirred in the dark at room temperature for 8 h. The crude product was purified as described earlier for 10−30 kDa nanocarriers. The pure nanocarriers were obtained as yellow flakes after freeze-drying and were characterized by GPC and MALDI-TOF.

*40 kDa.* Yield: 40 mg (79.3%). GPC: $t_R$ = 6.1 min (PEG-fluorescein) and 7.6 min (PEG-$NH_2$). MALDI-TOF ($m/z$): calculated, 42942.37 Da; observed, 43554.15 Da (PEG-fluorescein).

*60 kDa.* Yield: 32.9 mg (65.4%). GPC: $t_R$ = 5.6 min (PEG-fluorescein) and 6.8 min (PEG-$NH_2$). MALDI-TOF ($m/z$): calculated, 58119.37 Da; observed, 58867.61 Da (PEG-fluorescein).

*Cell Culture.* The 4T1 murine breast cancer cell line was a generous gift from Dr. Michael Reiss, The Cancer Institute of New Jersey (New Brunswick, NJ). The cells were maintained in Dulbecco's modified Eagle's medium (DMEM) supplemented with 10% fetal bovine serum (FBS), penicillin (200 units/mL), and streptomycin (200 mg/mL) at 37 °C in 5% $CO_2$ atmosphere. Cells with confluency less than 80% were used for animal inoculation.

*Animals.* Female balb/c mice (10-weeks old) were obtained from The Jackson Laboratory (Bar Harbor, ME). A protocol approved by the Rutgers University Institutional Animal Care and Use Committee was used for animal experiments. The animals were housed in an animal facility at the University, maintained on a 12 h light/dark cycle in a temperature-controlled environment, with food and water ad libitum. After acclimatization for one week, mice were injected subcutaneously into the abdominal area with 4T1 cells ($6.5 \times 10^5$ cells/mouse) suspended in serum-free medium. Seven to ten days after cell inoculation (average tumor weight: 0.09 g on sacrifice), abdominal hairs were removed under anesthesia with ketamine/xylazine cocktail (80/12 mg/kg), a day prior to the studies.

*Noninvasive Tumor Distribution Studies on a SkinSkan Spectrofluorometer.* The nanocarrier solutions (0.5 mM, saline) were injected intravenously into mice bearing tumors. Animals were monitored for signs of discomfort. Five to seven animals were used for each group unless indicated otherwise.

A series of in vivo fluorescence spectra were recorded from the marked tumor and a contralateral skin site before injection (blank) and at different time points after injection. The animals were anesthetized with isoflurane prior to each measurement and allowed to recover after the measurement. The spectra were collected on a fiber optic-based SkinSkan spectrofluorometer by placing the distal end of the fiber bundle (connected to a probe) in direct contact with the surface (tumor and control) under investigation. The fluorescence spectra were recorded in the range of 500−550 nm using 480 nm as the excitation wavelength, whereas the excitation spectra were recorded in the range of 220−500 nm using 515 nm (10−30 kDa) or 520 nm (40−60 kDa) as the emission wavelength. An increment of 0.5 nm, integration time of 0.5 s, and slit width of 0.5 mm were used to record the spectra. The instrument was calibrated prior to use, and DATAMAX software was used to control the instrument and acquire data.

*Noninvasive Tumor Distribution Studies on an IVIS 100 Imaging System.* The nanocarrier solutions (0.5 mM, saline) were administered intravenously to tumor bearing mice, as described earlier for SkinSkan studies. The animals were monitored for signs of discomfort. Three mice were used for each study group, and two untreated tumor-bearing mice were used as controls. A series of whole body animal images were recorded noninvasively at different time points. To record the images, animals were anesthetized with isoflurane prior to each measurement and allowed to recover after the measurement. The following instrument settings were used: level, high; $\lambda_{em}/\lambda_{exc}$, green fluorescent protein (GFP); bin, HR (4); field of vision (FOV), 25; aperture, f4; and shutter, 1 s.

*Ex Vivo Tissue Distribution Studies on a Fluorescence Plate Reader.* The mice were euthanized at 24 (10−60 kDa) and 96 h (40−60 kDa) after the injection. The blood samples were collected by cardiac puncture, and plasma was prepared and stored at −80 °C. Tumor, lung, spleen, liver, kidney, muscle, and heart were removed and stored at −80 °C. All tissues were weighed and homogenized in 10 volumes (w/v) of phosphate buffered saline (PBS) followed by centrifugation at 4 °C for 15 min (12000$g$). The fluorescence from the resulting supernatants was measured on a microplate reader using excitation and emission filters of 485 and 535 nm. The results were normalized with nanocarrier standard curves prepared in corresponding tissue homogenates. Five to seven animals were used unless indicated otherwise.

*Data Analysis.* Experimental values were expressed as mean ± standard deviation. One-way or two-way ANOVA and nonlinear regression analysis were conducted using GraphPad Prism v.4, and differences between individual groups were determined using Student's $t$ test (Microsoft Excel 2008), and Bonferroni and Tukey posthoc tests. Area under the curve ($AUC_{0-t}$) was calculated with PKSolver.[41]

## RESULTS

**Synthesis and Characterization of Fluorescein-Labeled PEG Nanocarriers.** PEG polymers do not show fluorescence and must be labeled to facilitate their detection. Fluorescein was used to label PEGs in this work because it is a green fluorescent dye that has been extensively used for covalently labeling peptides, proteins, and oligonucleotides. It has good water solubility, relatively high molar absorptivity, and excellent quantum yield.[42] Fluorescein-labeled nanocarriers, in the molecular weight range 10−60 kDa, were prepared by coupling fluorescein-5-maleimide and fluorescein-5-succinimidyl ester to PEG-thiol and PEG-amine, respectively (Scheme 1). The PEG-thiols (10, 20, and 30 kDa) were reacted with fluorescein-5-maleimide at room temperature in aqueous sodium phosphate buffer containing EDTA to obtain 10−30 kDa nanocarriers. EDTA was added to buffer to maintain thiols in a reduced state and prevent the formation of disulfide linkages. Similarly, the PEG-amines (40 and 60 kDa) were reacted with fluorescein-5-succinimidyl ester at room temperature in aqueous sodium phosphate buffer to obtain 40−60 kDa nanocarriers. All reactions were carried out in the dark, and nanocarriers were purified on Sephadex column using water as eluent. The nanocarrier yields were in the range of 65−80%, suggesting a highly efficient

**Scheme 1**[a]

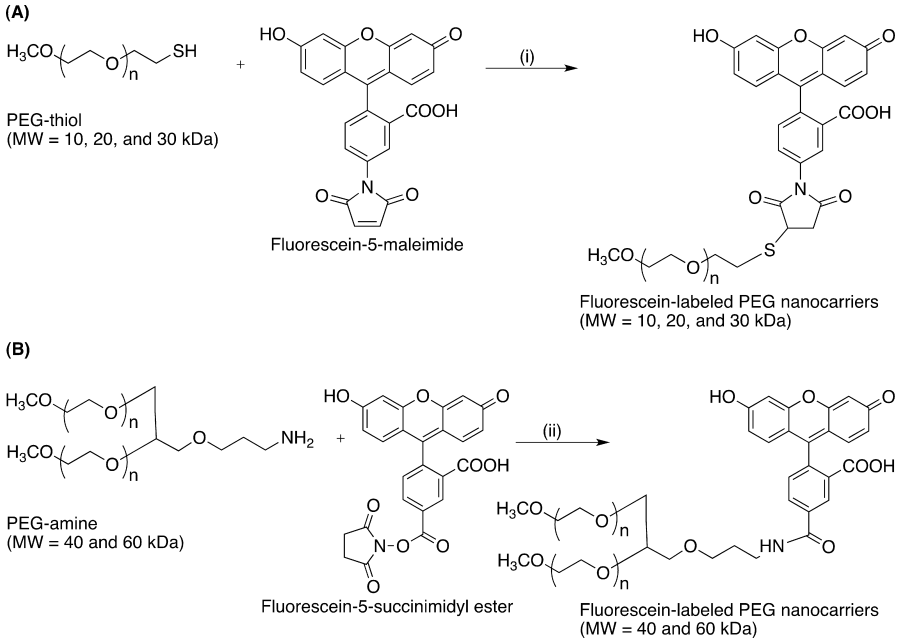


[a]Synthesis of fluorescein-labeled PEG nanocarriers: (A) 10, 20, and 30 kDa; and (B) 40 and 60 kDa. Reagents and conditions: (i) aqueous sodium phosphate buffer (0.1 M, pH, 7.4) containing EDTA (5 mM), room temperature, 8 h; and (ii) aqueous sodium phosphate buffer (0.1 M, pH, 8.0), room temperature, 8 h. Fluorescein is linked to PEG polymers through relatively stable thioether (10−30 kDa) or amide (40−60 kDa) bonds.

coupling. The fluorescein was conjugated to PEG using either the thioether (10−30 kDa) or amide (40−60 kDa) linkages, both relatively stable in vivo.[43]

The nanocarriers' purity was determined on a Breeze GPC system equipped with UV and refractive index (RI) detectors (see the Supporting Information). The retention times for unmodified PEG (10, 20, 30, 40, and 60 kDa) were obtained as 8.9, 8.3, 7.9, 7.6, and 6.8 min respectively, whereas the retention times for the corresponding PEG nanocarriers were 8.2, 7.4, 6.3, 6.1, and 5.6 min, respectively. Thus, the retention times for the nanocarriers were always slightly lower than for unmodified PEG because of the increase in their molecular weight after conjugation. All nanocarriers were obtained in high purity (≥85%), and unreacted dye was not detected in the chromatogram. The unmodified PEGs showed a peak in the RI panel but not the UV panel (480 nm), as they do not absorb at this wavelength, which is a characteristic for fluorescein. However upon conjugation with dye, all nanocarriers showed peaks in the RI as well as UV panels, indicating the covalent attachment of dye to PEGs. Finally, the nanocarriers were characterized by estimating their molecular weight on a MALDI-TOF mass spectrometer (see the Supporting Information). The molecular weights for 10−60 kDa nanocarriers were found as 10393.7, 21332.0, 31659.3, 43554.1, and 58867.6 Da, which were in agreement with calculated values of 10291.3, 20100.0, 28873.3, 42942.3, and 58119.37 Da, respectively.

To establish a correlation between the molecular weight of a PEG and its size, hydrodynamic radii of PEG polymers were measured using DLS. The hydrodynamic radii of 10, 20, 30, 40, and 60 kDa polymers were estimated as 4.894 ± 0.590, 6.568 ± 0.660, 8.230 ± 0.588, 9.175 ± 0.383, and 9.783 ± 0.676 nm, respectively. The hydrodynamic radii increased with an increase in molecular weight, but the increase was more prominent in the molecular weight range of 10−30 kDa than 30−60 kDa. The hydrodynamic radii were plotted against molecular weight (Figure 1), and data were fitted using the one phase exponential association equation ($R^2$ = 0.9135). The plot showed

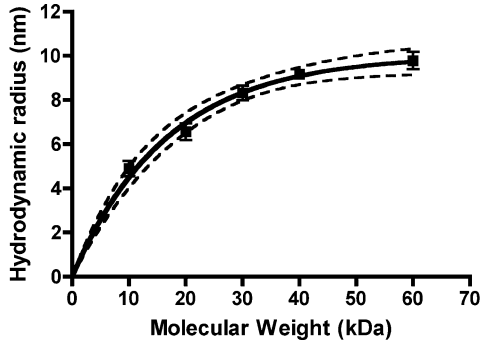


**Figure 1.** Plot of hydrodynamic radii vs molecular weight for PEG polymers. The data were fitted using a one-phase exponential association equation in GraphPad Prism v.4 software ($R^2$ = 0.9135). Each data point represents mean ± SD ($n$ = 3). The solid line indicates the best-fit line whereas the dashed line indicates the 95% confidence interval.

that increase in hydrodynamic radii with molecular weight was not linear, which is expected because of the fact that 10−30 kDa PEGs are linear but the 40−60 kDa PEGs are branched with two arms. As described earlier, molecular size of polymers is influenced by molecular weight, chemical nature, shape, and conformation in water.

**Noninvasive Tumor Distribution Studies Using a SkinSkan Spectrofluorometer.** The passive tumor distribution exhibited by nanocarriers was measured on a SkinSkan spectrofluorometer, which is specially designed to measure fluorescence from the surface of the skin. The SkinSkan comprises a distal probe connected to the instrument through fiber optic bundle, which transmits the excitation light to sample and


dx.doi.org/10.1021/mp2003913 | Mol. Pharmaceutics 2012, 9, 144−155

collects resulting fluorescence on a photomultiplier. The fluorescence is measured by placing a distal probe directly over the surface under investigation (e.g., tumor and contralateral skin site). This instrument has been previously used to detect and measure endogenous and exogenous fluorescence markers on the skin, with high sensitivity and precision for various applications.[39,44]

To assess the instrument's capability to collect fluorescence spectra from a highly scattered background source such as the skin, the 40 kDa nanocarrier was administered intravenously to a control mouse, and fluorescence spectra were recorded from skin surface before and after administration (Figure 2). The

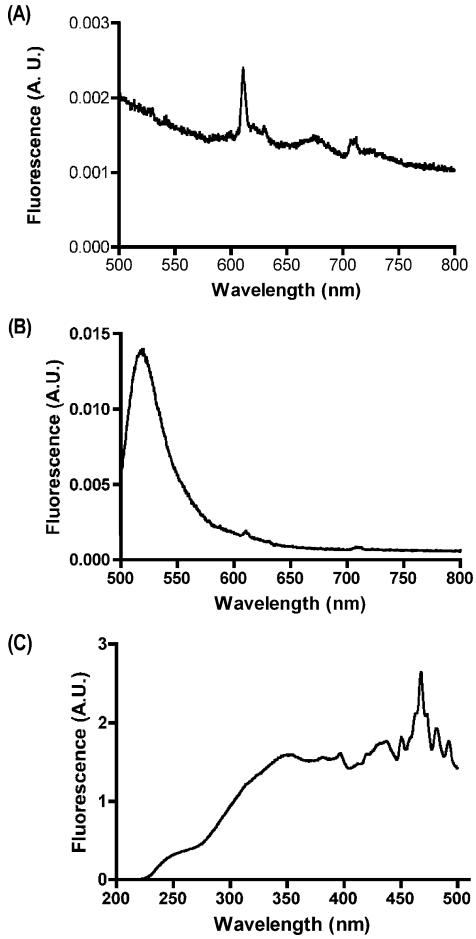


**Figure 2.** Fluorescence spectra obtained from the skin surface of a control mouse: (A) before injection; (B) 10 min after the injection of 40 kDa nanocarrier (intravenous, 0.5 mM); and (C) the excitation spectrum. The spectra were recorded using the excitation and emission wavelengths of 480 and 520 nm.

spectra recorded at the skin surface of a control animal showed low background in the 500−550 nm range where fluorescein is known to emit strongly (Figure 2A), even though a small peak was observed at 611 nm. Skin fluorescence increased rapidly (7.3 times at emission maxima) within minutes of nanocarrier administration (Figure 2B), and a fluorescence spectrum characteristic of fluorescein was obtained with emission peaking at 519 nm. Thus, PEGylation did not compromise the fluorescence properties of dye. In addition, the excitation spectra recorded from the skin's surface showed characteristic peaks at 350, 468, 482, and 492 nm, which were overlapping with the absorption spectra of fluorescein (Figure 2C). The presence of unperturbed excitation spectra points to the lack of undesirable dye interactions. Furthermore, the in vivo excitation and emission spectra obtained from the skin's surface were identical to spectra obtained in vitro (not shown).

The 4T1 model was used for in vivo studies because it is considered an appropriate animal model for mammary cancer due to its high tumorigenicity in mice and its ability to metastasize to multiple distant sites like the lymph nodes, liver, lung, brain and bone.[45] Aqueous nanocarrier solutions were prepared and administered intravenously to tumor-bearing female balb/c mice to investigate passive tumor distribution of nanocarriers. The tumor distribution was monitored using SkinSkan by measuring fluorescence spectra from the marked tumor and adjacent contralateral skin site, before and at different time points after injection (Figure 3).

The passive tumor distribution of 10 kDa nanocarrier was similar to that of the dermal control site. The signal intensity reached peak values within 30 min and then fell rapidly to become undetectable after 4 h (Figure 3). Unlike the 10 kDa nanocarrier, the 20 and 30 kDa nanocarriers showed higher tumor distribution as compared to control site. The 20 kDa nanocarriers reached peak levels within 1−3 h of administration, whereas the 30 kDa nanocarrier attained peak values within 1−5 h. The signal intensities then decreased continuously for both nanocarriers and became undetectable at control site at 24 and 48 h for 20 and 30 kDa nanocarriers, respectively, but remained strong in tumors for at least 72 h, indicating higher passive tumor distribution of these nanocarriers, compared to control site. As expected, the 40 and 60 kDa nanocarriers showed much higher tumor distribution than 10−30 kDa nanocarriers. The 40 and 60 kDa nanocarriers reached peak levels within 3−5 and 5−8 h, and then exhibited a continuous decrease. Contrary to 10−30 kDa nanocarriers, the signal intensity remained strong in tumors and control sites for at least 96 h, with signal intensity from tumor being always higher than that from control site.

Overall nanocarrier distribution followed the rank order 10 < 20 < 30 ≪ 40 ≪ 60 kDa. At 24 h, the 10 kDa nanocarrier was not detected in tumors contrary to 20−60 kDa nanocarriers. Also, the 30, 40, and 60 kDa nanocarriers showed 2.1, 5.3, and 4.1 times higher tumor distribution than 20 kDa nanocarrier. Similarly, at 96 h, the 10−30 kDa nanocarriers were not detected in tumors unlike the 40 and 60 kDa nanocarriers. The 60 kDa nanocarrier showed about 1.5 times higher tumor distribution than 40 kDa nanocarrier. Clearly, the PEG nanocarriers showed molecular weight-dependent passive distribution in tumors, with nanocarriers close to or above the renal exclusion limit (≥45 kDa for globular proteins) exhibiting much higher tumor distribution than those below it. By labeling PEGs with fluorescent dye, it was possible to detect and measure their passive tumor distribution noninvasively from the skin's surface.

**Noninvasive Tumor Distribution Studies Using an in Vivo Imaging System (IVIS 100).** The passive tumor distribution of PEG nanocarriers was further investigated using an IVIS 100 small animal imaging system (Figure 4). The nanocarriers were administered intravenously to tumor bearing mice, which were anesthetized at different time points to obtain whole body images (Figure 4A). The tumor distributions obtained by IVIS were compared to those measured using SkinSkan.

Compared to the control site, the 10 kDa nanocarrier showed no significant difference in tumor distribution. The signal intensity from tumor and control site decreased rapidly, and became undetectable in less than 24 h (Figure 4C). The 20 and 30 kDa

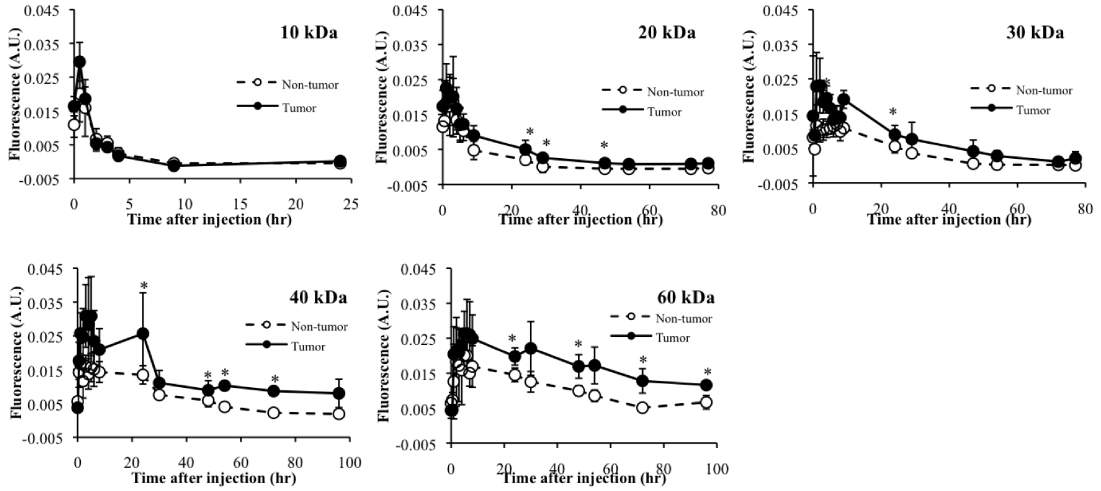


**Figure 3.** Passive tumor distribution of PEG nanocarriers measured noninvasively using a SkinSkan spectrofluorometer. Nanocarriers (0.5 mM) were intravenously administered to 4T1 tumor-bearing balb/c mice, and fluorescence spectra were collected from tumor and a contralateral skin ($\lambda_{exc}$, 480 nm; $\lambda_{em}$, 515 nm for 10−30 kDa and 520 nm for 40−60 kDa). Each column and error bar represents the mean ± SD ($n$ = 5−7). Individual comparisons between the groups were determined by Student's $t$ test using Microsoft Excel 2008. *: $p < 0.05$, tumor vs corresponding dermal control site.

nanocarriers showed slightly higher tumor distribution compared to control site, and both nanocarriers were detected in tumors for up to 48 h after the administration. The difference between the distribution of 20 and 30 kDa nanocarriers in tumors and the control site was found slightly lower from IVIS than SkinSkan, which could be due to the difference in instrument sensitivity/response. The 40 and 60 kDa nanocarriers showed significantly higher tumor distribution than control site, with tumor distribution of 60 kDa nanocarrier being higher than 40 kDa nanocarrier. Unlike 10−30 kDa nanocarriers, the 40 and 60 kDa nanocarriers were detected in tumors and the control site for at least 4-days (~96 h). Overall the results obtained from IVIS studies were in good agreement with the SkinSkan data.

**Passive Tumor Distribution vs Molecular Weight.** The data obtained from in vivo SkinSkan (Figure 3) and IVIS (Figure 4) were used to further evaluate passive distribution of nanocarriers in tumors. The $AUC_{0-t}$ values obtained using both methods were plotted against molecular weights of PEG nanocarrier (Figure 5). Good linear relationships were achieved between $AUC_{0-t}$ of SkinSkan or IVIS and nanocarrier molecular weights. The slope for SkinSkan and IVIS plots against molecular weights were 0.03054 and 0.001991, whereas the $R^2$ values were 0.9841 and 0.9298, respectively, implying molecular weight-dependent distribution of nanocarriers in tumors.

**Ex Vivo Tissue Distribution Studies Using a Fluorescence Plate Reader.** Ex vivo tissue distribution studies were carried out to corroborate results obtained from in vivo studies. The blood samples, tumors, and tissue samples such as liver, kidney, spleen, heart, lung, and abdominal muscle were collected at 24 (10−60 kDa) and 96 h (40−60 kDa) after injection, and PEG nanocarriers were quantified using a fluorescence plate reader (Figure 6). The analysis of various tissue homogenates showed that the maximum distribution of nanocarriers occurred in tumor, followed by lung, spleen, liver, kidney, muscle, and heart (Figure 6A). Relatively higher distribution of nanocarriers in the spleen, liver, and kidney (particularly the 40 and 60 kDa nanocarriers) indicates that, in addition to renal filtration, other elimination routes (e.g., liver uptake, immune system etc.) are involved in their removal from the body.

Similar to noninvasive SkinSkan and IVIS studies, the analysis of tumor homogenates showed that the tumor distribution of PEG nanocarriers is molecular weight-dependent (Figure 6B). At 24 h, tumor distribution was shown to follow the order 10 < 20 < 30 ≪ 40 ≪ 60 kDa. The 20−30 kDa and 40−60 kDa nanocarriers showed 2−3 and 11−13 times higher tumor distribution than 10 kDa nanocarrier. Unlike the 10−30 kDa nanocarriers, which were not detected in tumors at 96 h, the 40 and 60 kDa nanocarriers were detected in tumors even at 96 h. Interestingly, the tumor distribution of 40 kDa nanocarrier at 96 h was 2.7 times lower than 24 h, which was contrary to 60 kDa nanocarrier, where the tumor distribution continued to increase even at 96 h (1.5 times higher at 96 h than 24 h).

Furthermore, the tumor distribution of PEG nanocarriers correlated well with their plasma persistence, which at 24 h followed the order 10 < 20 < 30 ≪ 40 ≪ 60 kDa (Figure 6C). Compared to 10 kDa nanocarrier, the 20, 30, 40, and 60 kDa nanocarriers showed 4.8, 38.6, 105, and 235 times higher plasma persistence, respectively. The plasma levels for all nanocarriers decreased over time due to their slow elimination from the body (renal, hepatic, immune system), even though the 40 and 60 kDa nanocarriers remained detectable for up to 96 h. This is consistent with earlier studies that demonstrated that the longer plasma residence time of nanocarriers (mainly due to the decreased renal clearance) leads to higher passive distribution in tumors.[28,46] Thus, the tissue biodistribution studies corroborated the results obtained from noninvasive SkinSkan and IVIS studies.

**In Vivo and in Vitro Correlation.** The in vivo tumor distribution data (average fluorescence) were plotted against the ex vivo tumor distribution data (pmol/mg tumor) to establish a correlation between two methods (Figure 7). A linear correlation was obtained for the plots of in vivo tumor distribution obtained from SkinSkan and IVIS against the ex vivo tumor distribution obtained from the plate reader, with $R^2$ values of 0.9339 and 0.969, respectively (Figure 7). Correlation studies, similar to in vivo and ex vivo studies, were indicative of molecular weight-dependent passive distribution of PEG nanocarriers in tumor.


dx.doi.org/10.1021/mp2003913 | Mol. Pharmaceutics 2012, 9, 144−155

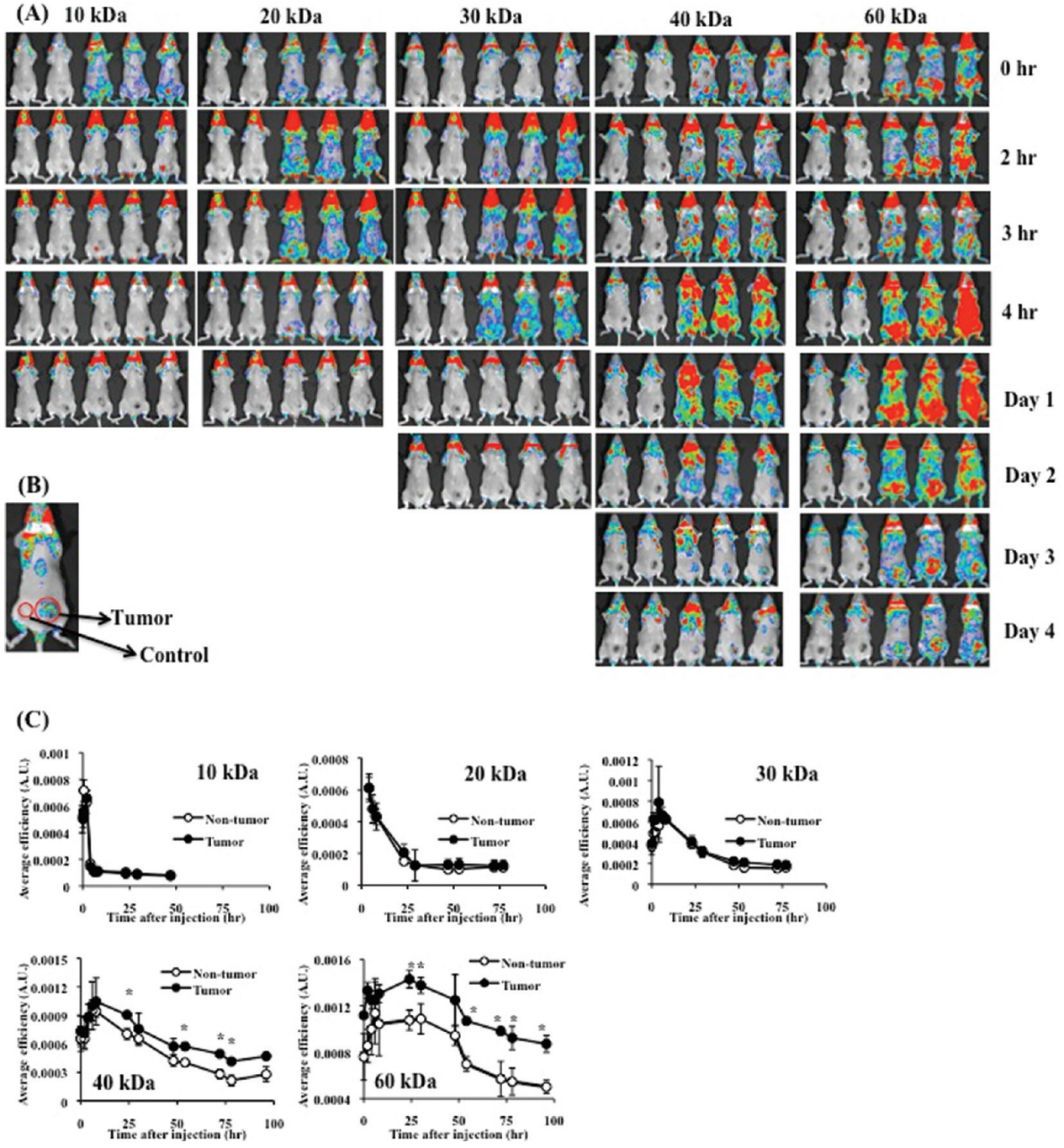


**Figure 4.** (A) Noninvasive images showing the passive tumor distribution of PEG nanocarriers. The images were obtained on an IVIS 100 imaging system using the excitation and emission filters corresponding to green fluorescent protein (GFP). The first two animals (balb/c mice with 4T1 tumor), starting from the left, were untreated (controls), whereas the remaining three animals were administered nanocarriers (0.5 mM) intravenously. (B) Regions of interest for tumor and control areas are shown in a mouse injected with 40 kDa nanocarrier for average efficient quantitation. (C) Plots of average fluorescence from tumor and control site at the skin's surface against time. Each point represents the mean ± SD ($n$ = 3). Individual comparisons between groups were determined by Student's $t$ test using Microsoft Excel 2008. *: $p < 0.01$, tumor vs corresponding control site.

## DISCUSSION

Polymeric nanocarriers were initially used to deliver proteins, which though potent show poor stability, short plasma half-life, and high immunogenicity.[47,48] A relevant example is recombinant interferon-$\alpha$ (IFN), used to treat chronic hepatitis C, which is rapidly absorbed ($t_{1/2}$: 2.3 h) and reaches peak plasma levels in 1−8 h before falling (elimination $t_{1/2}$: 3−8 h) to become undetectable within 24 h.[13] The clinically approved PEG-Intron (peginterferon $\alpha$-2b),[14,15] which is modified with a 12 kDa linear PEG, shows absorption and elimination half-lives ($t_{1/2}$) of 7 h and 4 days, whereas the Pegasys (peginterferon $\alpha$-2a),[13] which is modified with a 40 kDa branched PEG, shows the absorption and elimination half-lives ($t_{1/2}$) of 50 h and 11 days. Both PEGylated interferons, with safety profiles similar to that of interferon, are administered subcutaneously once weekly with ribavirin instead of three times a week, for unmodified interferon.


dx.doi.org/10.1021/mp2003913 | Mol. Pharmaceutics 2012, 9, 144−155

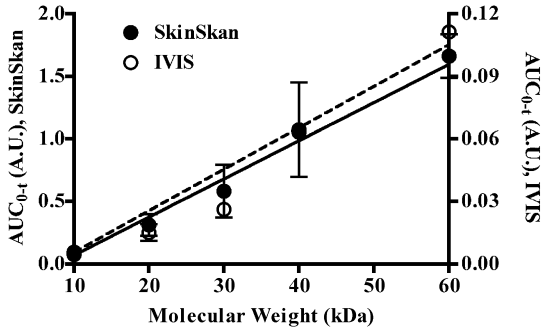


**Figure 5.** Molecular weight-dependent tumor distribution of PEG nanocarriers. The $AUC_{0-t}$ obtained from SkinSkan (solid) and IVIS (dashed) studies, as depicted in Figures 3 and 4, were plotted against nanocarriers molecular weight. Linear relationships were obtained for SkinSkan and IVIS plots, with slopes of 0.03054 and 0.001991, respectively; and $R^2$ of 0.9841 and 0.9298, respectively. One-way ANOVA with multiple Tukey's posttests were performed. Except for 10 vs 20 kDa and 20 vs 30 kDa, all groups measured using SkinSkan showed significant differences in $AUC_{0-t}$ ($p < 0.05$). All groups measured using IVIS were significantly different from each other ($P < 0.01$).

Polymers have been shown to target anticancer drugs passively (without targeting groups) to tumors. Matsumura and Maeda were the first to observe higher distribution of polymer conjugates (SMANCS) in tumors.[8−10] They used $^{51}$Cr-labeled proteins, of various molecular weights (12−160 kDa), to elucidate the general mechanism for passive distribution of SMANCS in tumors and found that the higher tumor distribution was a result of unique vascular characteristics and lack of lymphatic drainage in tumors.[28] This phenomenon came to be known as the enhanced permeability and retention (EPR)[29,30] effect. It occurs because the tight junctions between endothelial cells of microvessels measure around 2 nm[49] (6 nm in kidney, liver, spleen),[50] whereas the pore size of tumor microvessels varies from 100 to 1200 nm.[51] Therefore, polymers are able to extravasate into tumors, and not normal tissues, where they are retained because of slow venous return and poor lymphatic drainage.

The Kopecek and Duncan groups developed the PK1 (HPMA−gly-phe-leu-gly−doxorubicin), which contains doxorubicin (~8.5 wt %) conjugated to HPMA copolymer ($M_w$ ~30 kDa) via a cathepsin B-sensitive tetrapeptide linker.[21,22] It showed a maximum-tolerated dose (MTD) of 320 mg/m$^2$ in phase I trial, 4- to 5-fold higher than the normal safe dose of the free drug, and no cardiotoxicity typical of anthracyclines up to the cumulative dose of 1680 mg/m$^2$. The conjugate showed prolonged plasma half-life ($t_{1/2\alpha}$ = 1.8 h) and antitumor activity consistent with EPR-mediated tumor targeting in chemotherapy resistant/refractory patient, and at low doses (80−180 mg/m$^2$). Another interesting polymer conjugate, currently in phase III clinical trial, is CT-2103 (OPAXIO),[26] which is obtained by conjugating paclitaxel (37 wt %) to cathepsin B-sensitive biodegradable PGA polymer ($M_w$ ~17 kDa) via degradable ester linkages, giving an overall molecular weight of 49 kDa. It showed a MTD of 233 mg/m$^2$ in phase I trial, and promising response in patients with mesothelioma, renal cell carcinoma, non-small cell lung cancer (NSCLC), and paclitaxel-resistant ovarian cancer.

Initially water-soluble polymers like HPMA, PGA, PEG, and dextran were used to prepare polymer conjugates of anticancer drug, but later more complex branched polymers, dendrimers, dendronized polymers, and self-assembling polymers were also

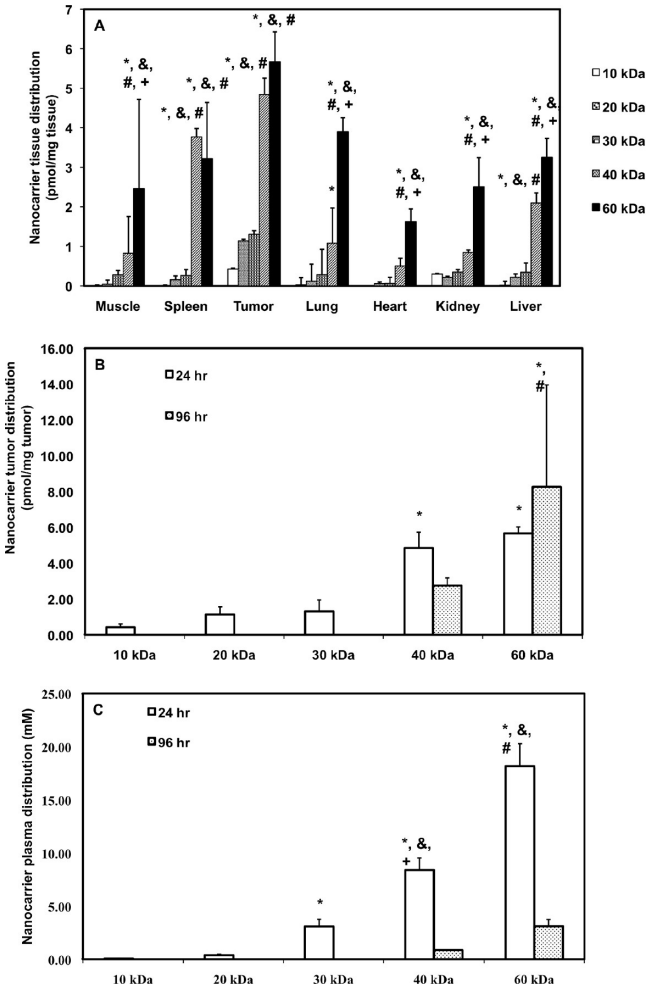


**Figure 6.** Ex vivo distribution studies: (A) tissue distribution at 24 h; (B) tumor distribution at 24 and 96 h; and (C) plasma distribution at 24 and 96 h. PEG nanocarriers (0.5 mM) were intravenously administered to balb/c mice bearing 4T1 tumors, and animals were euthanized to collect tissues. Each column and error bar represents the mean ± SD ($n$ = 5−7). The statistical analyses were carried out using GraphPad Prism v.4 as follows: (A) Two-way ANOVA and individual comparison between the groups were determined using Bonferroni posttests. The statistically significant groups ($p < 0.05$, 60 kDa vs other nanocarriers) are marked as * (10 kDa); & (20 kDa); # (30 kDa); and + (40 kDa). (B) One-way ANOVA and individual comparison between the groups were determined using Tukey posttests. The statistically significant groups ($p < 0.05$, 60 kDa vs other nanocarriers are marked as * (10, 20, or 30 kDa) and # (40 kDa at 96 h). (C) One-way ANOVA and comparison between the groups were determined using Tukey posttests. The statistically significant groups ($p < 0.05$, 60 kDa vs other nanocarriers) are denoted by * (10 or 20 kDa); & (30 kDa); # (40 kDa); and + (nanocarriers at 96 h).

developed.[1,2] Due to the pioneering work of Prof. Frank Davis at Rutgers,[52,53] PEGs are considered the most useful polymer for clinical applications. PEGs are made of chemically inert polyether backbone; are nontoxic, nonimmunogenic, and nonbiodegradable; and show excellent solubility in aqueous media.[17,54,55]

The aim of present studies was to investigate EPR-mediated passive tumor distribution of PEG nanocarriers by noninvasive dermal imaging, as a tool to screen nanocarriers for tumor targeting. PEGs of varying molecular weights (10−60 kDa) labeled with fluorescein were administered to tumor-bearing


dx.doi.org/10.1021/mp2003913 | Mol. Pharmaceutics 2012, 9, 144−155

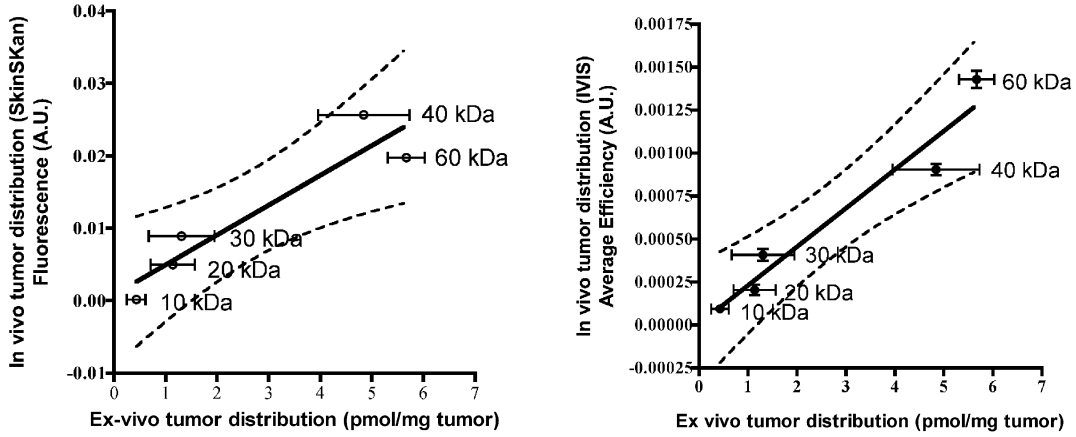


**Figure 7.** Correlation between the in vivo and ex vivo tumor distribution of PEG nanocarriers: (A) average fluorescence (SkinSkan) vs ex vivo tumor distribution (pmol/mg tumor); $R^2$ = 0.9339; and (B) average fluorescence (IVIS) vs ex vivo tumor distribution (pmol/mg tumor); $R^2$ = 0.969. Data are reported as mean ± SD ($n$ = 5−7). The solid line indicates the best-fit line whereas the dashed line indicates the 95% confidence interval.

mice, and passive tumor distribution was monitored noninvasively by measuring the fluorescence from the tumor and contralateral skin site using SkinSkan and IVIS. Fluorescein emits in the visible range (400−700 nm), and such probes, even though useful, suffer from limitations like poor penetration of light (only a few millimeters) and high autofluorescence from tissues.[35] To improve the sensitivity of detection, near-infrared (NIR) probes, emitting in the NIR region (700−1400 nm), are employed. These probes exhibit high sensitivity of detection because the NIR light has high penetration depth (several centimeters) and autofluorescence from tissues is minimal in this region.[35] Moreover, the emission spectra are typically narrow and therefore useful in multicolor imaging.

At 24 h, the 10 kDa nanocarrier was not detected in tumors or the control site, whereas 20−60 kDa nanocarriers exhibited higher tumor distribution than the control site. The 30, 40, and 60 kDa nanocarriers showed 2.1, 5.3, and 4.1 times higher tumor distribution than the 20 kDa nanocarrier. At 96 h, the 60 kDa nanocarrier showed 1.5 times higher tumor distribution than the 40 kDa nanocarrier. The PEG nanocarriers showed molecular weight-dependent passive distribution in tumor in the order 10 < 20 < 30 ≪ 40 ≪ 60 kDa, which is not unexpected because the DLS studies showed that the hydrodynamic radii of PEG polymers increased with an increase in molecular weight. However, this increase in radii was not linear, as both the molecular weight and polymer structure were found to influence the size. The animal images obtained on an IVIS gave similar results. The plots of $AUC_{0-t}$ obtained from SkinSkan and IVIS against nanocarriers' molecular weight also demonstrated molecular weight-dependent distribution of nanocarriers in tumor, and this was further validated by the ex vivo tissue distribution studies.

The tissue distribution studies also showed a correlation between the tumor distribution of nanocarriers and their plasma concentrations, which at 24 h followed the rank order 10 < 20 < 30 ≪ 40 ≪ 60 kDa. Significant amounts of the nanocarriers were present in spleen, liver, and kidney indicating the involvement of other elimination routes (e.g., liver uptake, immune system etc.) in their removal from body.[56] Kaminskas et al. observed that PEGylated dendrimers with molecular weight >30 kDa showed poor renal clearance and extended elimination half-lives, whereas those with molecular weight <20 kDa were rapidly cleared in urine.[57] This is very different from proteins, where the renal filtration threshold is around 40−60 kDa; and proteins with molecular weight >70 kDa are removed by other elimination routes.[58,59]

Earlier studies have shown that an increase in molecular weight of proteins increases their plasma half-life, which in turn leads to higher passive tumor distribution.[28,29] Maeda and co-workers used $^{51}$Cr-labeled proteins, of different molecular weight, to investigate their passive distribution behavior in tumors.[28] The plasma half-life of NCS ($M_w$: 12 kDa) was found to be only 2 min, whereas the plasma half-life of SMANCS ($M_w$: 17 kDa) was 18 min (9 times higher). Other proteins such as chicken ovomucoid ($M_w$: 29 kDa), albumins ($M_w$: 68 kDa) from bovine and mouse, and IgG ($M_w$: 150 kDa) showed plasma half-lives of 6, 60, 180, and 72 min, respectively. The peculiar behavior of ovomucoid or IgG is due to the fact that each protein has a unique conformation and charge, and is also subject to denaturation and degradation. The ratio of protein concentration in tumor to that in blood (T/B) of 1 or 5 was not observed for NCS, but was observed for SMANCS in 3.2 or 19 h. The high molecular weight protein like IgG attained these values in 15.3 or 72 h. Authors also observed significant distribution in liver and spleen besides tumor.

Seymour et al. investigated the passive tumor distribution of HPMA−drug conjugates ($M_w$: 22−778 kDa) in subcutaneous Sarcoma 180 and B16F10 melanoma models.[60] The plasma half-life of HPMA copolymers was found to be molecular weight-dependent. The copolymer with $M_w$ of 22 kDa exhibited plasma half-life of <10 min, whereas the copolymer with $M_w$ of 40 kDa exhibited plasma half-life of <30 min. Copolymers of higher molecular weights showed plasma half-lives in the range 20−24 h. At 24 h, the copolymer fractions with $M_w$ of 22 and 40 kDa did not show progressive distribution in tumors, but the copolymers with high molecular weight (≥78 kDa) showed progressive distribution in tumors, depending on their molecular weight. The T/B ratio in Sarcoma 180 was always greater than B16F10, and low distributions were observed in liver and spleen, unlike the findings of Maeda and co-workers.[28] The authors also investigated high molecular weight proteins for comparison and found that proteins show rapid loss from the bloodstream and less efficient distribution in tumors, compared to polymer of similar molecular weight.

Similar to earlier studies by Maeda[28] and Seymour,[60] PEG nanocarriers investigated here showed molecular weight-dependent passive distribution in tumors, largely due to an increase in plasma residence time resulting from decrease in

renal clearance. Contrary to Seymour's[60] work, where it was shown that HPMA with $M_w$ ≥78 kDa exhibited the EPR effect, the current study shows that PEG nanocarriers ≥40 kDa exhibit the EPR effect. In terms of size, nanocarriers obtained from polymers with hydrodynamic radii of ≥8 nm exhibited the EPR effect. Seymour et al.[60] reported little distribution in liver and spleen, but in the current study significant distribution was observed in liver, spleen, and kidney, similar to findings reported by Maeda and co-workers.[28] The difference in results could be explained by peculiar behavior of hydrated PEG molecules (see below).

Other high molecular weight molecules like plasma albumins (70 kDa), transferrin (90 kDa), IgG (150 kDa), etc. also show EPR-mediated tumor targeting,[30] but PEGs provide certain distinct advantages. PEG displays a coiled/extended conformation unlike proteins, which exhibit a compact and globular structure. They coordinate 2−3 water molecules per ethylene oxide unit when fully hydrated, which increases their apparent molecular weight 5−10 times higher than corresponding globular protein of comparable mass, as verified by GPC.[61] The extended surface of the conjugated moiety (protein/drugs) is enclosed within this large hydrodynamic volume, which prevents degradation, uptake by the RES, renal clearance, and reduces immunogenicity.

## CONCLUSION

In conclusion, the passive tumor distribution of PEG nanocarriers of varying molecular weights (10−60 kDa) was measured by noninvasive dermal imaging using the SkinSkan spectrofluorometer and IVIS imaging system. The nanocarriers labeled with fluorescein were administered to tumor-bearing mice, and the in vivo fluorescence was measured from the tumor and a contralateral skin site. Tumor distribution was found to be molecular weight-dependent, as it increased with an increase in molecular weight of nanocarriers (10 < 20 < 30 ≪ 40 ≪ 60 kDa). The 10 kDa nanocarrier was rapidly removed by renal filtration and did not show the EPR effect. The 20 and 30 kDa nanocarriers showed slightly higher EPR-based tumor distribution, whereas the 40 and 60 kDa nanocarriers with molecular weight close to or above the renal threshold, which for globular proteins is ≥45 kDa, showed significantly higher passive tumor distribution. In terms of size, nanocarriers obtained from polymer with hydrodynamic radii of ≥8 nm exhibited more prominent EPR effect. Furthermore, tumor distribution was found to correlate with the plasma half-life of nanocarriers, which also increased with an increase in molecular weight. In addition, the whole-body animal images obtained noninvasively on an IVIS 100 also confirmed the higher distribution of nanocarriers in tumor, and their molecular weight dependence. It should be mentioned that tumor size also influences passive distribution within the tumor, a fact that has not been investigated in this study but could be the subject of future studies. The ex vivo tissue distribution studies validated the results obtained from SkinSkan and IVIS studies and showed that, besides tumor, significant nanocarrier distribution occurred in lung, spleen, liver, and kidney. Thus, the unique capability of the SkinSkan spectrofluorometer to measure fluorescence from highly scattered background, like skin, was employed to monitor the passive tumor distribution of macromolecular nanocarriers. The method used in this work is advantageous because it is noninvasive and direct, and it does not involve cumbersome extraction procedures. This method may potentially be useful for high throughput screening of tumor-targeted polymer diagnostics and therapeutics in heterotopic tumor model.

## ASSOCIATED CONTENT

### Supporting Information

The GPC profiles and MALDI-TOF mass spectra of PEG nanocarriers and DLS profiles of unmodified polymers. This material is available free of charge via the Internet at http://pubs.acs.org.

## AUTHOR INFORMATION


### Corresponding Author

*Department of Pharmaceutics, Ernest Mario School of Pharmacy, Rutgers, The State University of New Jersey, 160 Frelinghuysen Road, Piscataway, NJ 08854, United States. Phone: (732) 445-3831 ext 213. Fax: (732) 445-4271. E-mail: sinko@rci.rutgers.edu.

### Author Contributions

†Y.S. and D.G. contributed equally to this work.


## ACKNOWLEDGMENTS

This work was supported by the grants from the United States Army Medical Research and Materiel Command (W81XWH-05-1-0342) and NIH HIT-IT (R01AI084137-01). We also thank Analytical Cytometry Image Analysis (AC/IA) Core Facility and Prof. Arash Hatefi at Rutgers University School of Pharmacy for providing access to IVIS 100 imaging system and Malvern Zetasizer Nano ZS, respectively.

## REFERENCES


(1) Duncan, R. Polymer conjugates as anticancer nanomedicines. *Nat. Rev. Cancer* **2006**, *6* (9), 688−701.

(2) Haag, R.; Kratz, F. Polymer therapeutics: concepts and applications. *Angew. Chem., Int. Ed.* **2006**, *45* (8), 1198−215.

(3) Vicent, M. J.; Duncan, R. Polymer conjugates: nanosized medicines for treating cancer. *Trends Biotechnol.* **2006**, *24* (1), 39−47.

(4) Duncan, R. The dawning era of polymer therapeutics. *Nat. Rev. Drug Discovery* **2003**, *2* (5), 347−60.

(5) Dhal, P. K.; Holmes-Farley, S. R.; Huval, C. C.; Jozefiak, T. H. Polymers as Drugs. *Adv. Polym. Sci.* **1996**, *192*, 9−58.

(6) Nakanishi, T.; Fukushima, S.; Okamoto, K.; Suzuki, M.; Matsumura, Y.; Yokoyama, M.; Okano, T.; Sakurai, Y.; Kataoka, K. Development of the polymer micelle carrier system for doxorubicin. *J. Controlled Release* **2001**, *74* (1−3), 295−302.

(7) Pack, D. W.; Hoffman, A. S.; Pun, S.; Stayton, P. S. Design and development of polymers for gene delivery. *Nat. Rev. Drug Discovery* **2005**, *4* (7), 581−93.

(8) Maeda, H.; Takeshita, J.; Kanamaru, R. A lipophilic derivative of neocarzinostatin. A polymer conjugation of an antitumor protein antibiotic. *Int. J. Pept. Protein Res.* **1979**, *14* (2), 81−7.

(9) Maeda, H.; Ueda, M.; Morinaga, T.; Matsumoto, T. Conjugation of poly(styrene-co-maleic acid) derivatives to the antitumor protein neocarzinostatin: pronounced improvements in pharmacological properties. *J. Med. Chem.* **1985**, *28* (4), 455−61.

(10) Maeda, H.; Matsumoto, H.; Konno, S.; Iwai, K.; Ueda, A. Tailor-making of protein drugs by polymer conjugation for tumor targeting: A brief review on SMANCS. *J. Protein Chem.* **1984**, *3*, 181−93.

(11) Levy, Y.; Hershfield, M. S.; Fernandez-Mejia, C.; Polmar, S. H.; Scudiery, D.; Berger, M.; Sorensen, R. U. Adenosine deaminase deficiency with late onset of recurrent infections: response to treatment with polyethylene glycol-modified adenosine deaminase. *J. Pediatr.* **1988**, *113* (2), 312−7.

(12) Graham, M. L. Pegaspargase: a review of clinical studies. *Adv. Drug Delivery Rev.* **2003**, *55* (10), 1293−302.

(13) Rajender Reddy, K.; Modi, M. W.; Pedder, S. Use of peginterferon alfa-2a (40 KD) (Pegasys) for the treatment of hepatitis C. *Adv. Drug Delivery Rev.* **2002**, *54* (4), 571−86.
(14) Bailon, P.; Palleroni, A.; Schaffer, C. A.; Spence, C. L.; Fung, W. J.; Porter, J. E.; Ehrlich, G. K.; Pan, W.; Xu, Z. X.; Modi, M. W.; Farid, A.; Berthold, W.; Graves, M. Rational design of a potent, long-lasting form of interferon: a 40 kDa branched polyethylene glycol-conjugated interferon alpha-2a for the treatment of hepatitis C. *Bioconjugate Chem.* **2001**, *12* (2), 195−202.
(15) Wang, Y. S.; Youngster, S.; Grace, M.; Bausch, J.; Bordens, R.; Wyss, D. F. Structural and biological characterization of pegylated recombinant interferon alpha-2b and its therapeutic implications. *Adv. Drug Delivery Rev.* **2002**, *54* (4), 547−70.
(16) Sundy, J. S.; Becker, M. A.; Baraf, H. S.; Barkhuizen, A.; Moreland, L. W.; Huang, W.; Waltrip, R. W. 2nd; Maroli, A. N.; Horowitz, Z. Reduction of plasma urate levels following treatment with multiple doses of pegloticase (polyethylene glycol-conjugated uricase) in patients with treatment-failure gout: results of a phase II randomized study. *Arthritis Rheum.* **2008**, *58* (9), 2882−91.
(17) Harris, J. M.; Chess, R. B. Effect of pegylation on pharmaceuticals. *Nat. Rev. Drug Discovery* **2003**, *2* (3), 214−21.
(18) Ringsdorf, H. Structure and properties of pharmacologically active polymers. *J. Polym. Sci., Polymer Symp* **1975**, *51*, 135−153.
(19) Gros, L.; Rinsdorf, H.; Schupp, H. Polymeric antitunor agents on a molecular and cellular level. *Angew. Chem., Int. Ed. Engl.* **1981**, *20*, 305−325.
(20) Duncan, R. N-(2-Hydroxypropyl)methacrylamide copolymer conjugates. In *Polymeric drug delivery system*; Kwon, G. S., Ed.; Marcel Dekker: New York, NY, 2005; pp 1−92.
(21) Kopecek, J.; Kopeckova, P.; Minko, T.; Lu, Z. HPMA copolymer-anticancer drug conjugates: design, activity, and mechanism of action. *Eur. J. Pharm. Biopharm.* **2000**, *50* (1), 61−81.
(22) Vasey, P. A.; Kaye, S. B.; Morrison, R.; Twelves, C.; Wilson, P.; Duncan, R.; Thomson, A. H.; Murray, L. S.; Hilditch, T. E.; Murray, T.; Burtles, S.; Fraier, D.; Frigerio, E.; Cassidy, J. Phase I clinical and pharmacokinetic study of PK1 [N-(2-hydroxypropyl)methacrylamide copolymer doxorubicin]: first member of a new class of chemotherapeutic agents-drug-polymer conjugates. Cancer Research Campaign Phase I/II Committee. *Clin. Cancer Res.* **1999**, *5* (1), 83−94.
(23) Meerum Terwogt, J. M.; ten Bokkel Huinink, W. W.; Schellens, J. H. M.; Schot, M.; Mandjes, I. A. M.; Zurlo, M. G.; Rocchetti, M.; Rosing, H.; Koopman, F.; Beijnen, J. H. Phase I clinical and pharmacokinetic study of PNU166945, a novel water soluble polymer-conjugated prodrug of paclitaxel. *Anti-Cancer Drugs* **2001**, *12*, 315−23.
(24) Bissett, D.; Cassidy, J.; de Bono, J. S.; Muirhead, F.; Main, M.; Robson, L.; Fraier, D.; Magne, M. L.; Pellizzoni, C.; Porro, M. G.; Spinelli, R.; Speed, W.; Twelves, C. Phase I and pharmacokinetic (PK) study of MAG-CPT (PNU 166148): a polymeric derivative of camptothecin (CPT). *Br. J. Cancer* **2004**, *91* (1), 50−5.
(25) Rowinsky, E. K.; Rizzo, J.; Ochoa, L.; Takimoto, C. H.; Forouzesh, B.; Schwartz, G.; Hammond, L. A.; Patnaik, A.; Kwiatek, J.; Goetz, A.; Denis, L.; McGuire, J.; Tolcher, A. W. A phase I and pharmacokinetic study of pegylated camptothecin as a 1-h infusion every 3 weeks in patients with advanced solid malignancies. *J. Clin. Oncol.* **2003**, *21* (1), 148−57.
(26) Sabbatini, P.; Aghajanian, C.; Dizon, D.; Anderson, S.; Dupont, J.; Brown, J. V.; Peters, W. A.; Jacobs, A.; Mehdi, A.; Rivkin, S.; Eisenfeld, A. J.; Spriggs, D. Phase II study of CT-2103 in patients with recurrent epithelial ovarian, fallopian tube, or primary peritoneal carcinoma. *J. Clin. Oncol.* **2004**, *22* (22), 4523−31.
(27) Bhatt, R.; de Vries, P.; Tulinsky, J.; Bellamy, G.; Baker, B.; Singer, J. W.; Klein, P. Synthesis and in vivo antitumor activity of poly(l-glutamic acid) conjugates of 20S-camptothecin. *J. Med. Chem.* **2003**, *46* (1), 190−3.
(28) Matsumura, Y.; Maeda, H. A new concept for macromolecular therapeutics in cancer chemotherapy: mechanism of tumoritropic accumulation of proteins and the antitumor agent smancs. *Cancer Res.* **1986**, *46* (12Part 1), 6387−92.
(29) Maeda, H.; Sawa, T.; Konno, T. Mechanism of tumor-targeted delivery of macromolecular drugs, including the EPR effect in solid tumor and clinical overview of the prototype polymeric drug SMANCS. *J. Controlled Release* **2001**, *74* (1−3), 47−61.
(30) Iyer, A. K.; Khaled, G.; Fang, J.; Maeda, H. Exploiting the enhanced permeability and retention effect for tumor targeting. *Drug Discovery Today* **2006**, *11* (17−18), 812−8.
(31) Chao, P.; Deshmukh, M.; Kutscher, H. L.; Gao, D.; Rajan, S. S.; Hu, P.; Laskin, D. L.; Stein, S.; Sinko, P. J. Pulmonary targeting microparticulate camptothecin delivery system: anticancer evaluation in a rat orthotopic lung cancer model. *Anticancer Drugs* **2010**, *21* (1), 65−76.
(32) Kutscher, H. L.; Chao, P.; Deshmukh, M.; Sundara Rajan, S.; Singh, Y.; Hu, P.; Joseph, L. B.; Stein, S.; Laskin, D. L.; Sinko, P. J. Enhanced passive pulmonary targeting and retention of PEGylated rigid microparticles in rats. *Int. J. Pharm.* **2010**, *402* (1−2), 64−71.
(33) Kutscher, H. L.; Chao, P.; Deshmukh, M.; Singh, Y.; Hu, P.; Joseph, L. B.; Reimer, D. C.; Stein, S.; Laskin, D. L.; Sinko, P. J. Threshold size for optimal passive pulmonary targeting and retention of rigid microparticles in rats. *J. Controlled Release* **2010**, *143* (1), 31−7.
(34) Andersson-Engels, S.; Klinteberg, C.; Svanberg, K.; Svanberg, S. In vivo fluorescence imaging for tissue diagnostics. *Phys. Med. Biol.* **1997**, *42* (5), 815−24.
(35) Adams, K. E.; Ke, S.; Kwon, S.; Liang, F.; Fan, Z.; Lu, Y.; Hirschi, K.; Mawad, M. E.; Barry, M. A.; Sevick-Muraca, E. M. Comparison of visible and near-infrared wavelength-excitable fluorescent dyes for molecular imaging of cancer. *J. Biomed. Opt.* **2007**, *12* (2), 024017.
(36) Yang, Y.; Katz, A.; Celmer, E. J.; Zurawska-Szczepaniak, M.; Alfano, R. R. Fundamental Differences of excitation spectrum between malignant and benign breast tissues. *Photochem. Photobiol.* **1997**, *66*, 518−22.
(37) Ramanujam, N. Fluorecence spectroscopy of neoplastic and non-neoplastic tissues. *Neoplasia* **2000**, *2*, 89−117.
(38) Zeng, H.; MacAulay, C.; McLean, D. I.; Palcic, B. Spectroscopic and microscopic characteristics of human skin autofluorescence emission. *Photochem. Photobiol.* **1995**, *61* (6), 639−45.
(39) Brancaleon, L.; Durkin, A. J.; Tu, J. H.; Menaker, G.; Fallon, J. D.; Kollias, N. In vivo fluorescence spectroscopy of nonmelanoma skin cancer. *Photochem. Photobiol.* **2001**, *73* (2), 178−83.
(40) Svanberg, K.; Wang, I.; Colleen, S.; Idvall, I.; Ingvar, C.; Rydell, R.; Jocham, D.; Diddens, H.; Bown, S.; Gregory, G.; Montan, S.; Andersson-Engels, S.; Svanberg, S. Clinical multi-colour fluorescence imaging of malignant tumours--initial experience. *Acta Radiol.* **1998**, *39* (1), 2−9.
(41) Zhang, Y.; Huo, M.; Zhou, J.; Xie, S. PKSolver: An add-in program for pharmacokinetic and pharmacodynamic data analysis in Microsoft Excel. *Comput. Methods Programs Biomed.* **2010**, *99* (3), 306−14.
(42) Haugland, R. P. Fluorophores and their amine-reactive derivatives. In *Handbook of fluorescent probes and research products*, 9th ed.; Molecular Probes, Inc.: Eugene, OR, 2002; pp 7−78.
(43) Singh, Y.; Spinelli, N.; Defrancq, E. Chemical strategies for oligonucleotide-conjugate synthesis. *Curr. Org. Chem.* **2008**, *12*, 263−90.
(44) Breslin, T. M.; Xu, F.; Palmer, G. M.; Zhu, C.; Gilchrist, K. W.; Ramanujam, N. Autofluorescence and diffuse reflectance properties of malignant and benign breast tissues. *Ann. Surg. Oncol.* **2004**, *11* (1), 65−70.
(45) Pulaski, B. A.; Ostrand-Rosenberg, S. Mouse 4T1 breast tumor model. *Curr. Protoc. Immunol.* **2001**, Chapter 20, Unit 20.2.
(46) Yang, B. B.; Lum, P. K.; Hayashi, M. M.; Roskos, L. K. Polyethylene glycol modification of filgrastim results in decreased renal clearance of the protein in rats. *J. Pharm. Sci.* **2004**, *93* (5), 1367−73.
(47) Leader, B.; Baca, Q. J.; Golan, D. E. Protein therapeutics: a summary and pharmacological classification. *Nat. Rev. Drug Discovery* **2008**, *7* (1), 21−39.
(48) Frokjaer, S.; Otzen, D. E. Protein drug stability: a formulation challenge. *Nat. Rev. Drug Discovery* **2005**, *4* (4), 298−306.
(49) Bundgaard, M. Transport pathways in capillaries--in search of pores. *Annu. Rev. Physiol.* **1980**, *42*, 325−36.

(50) Simionescu, N.; Simionescu, M.; Palade, G. E. Open junctions in the endothelium of the postcapillary venules of the diaphragm. *J. Cell Biol.* **1978**, *79* (1), 27−44.
(51) Hobbs, S. K.; Monsky, W. L.; Yuan, F.; Roberts, W. G.; Griffith, L.; Torchilin, V. P.; Jain, R. K. Regulation of transport pathways in tumor vessels: role of tumor type and microenvironment. *Proc. Natl. Acad. Sci. U.S.A.* **1998**, *95* (8), 4607−12.
(52) Abuchowski, A.; van Es, T.; Palczuk, N. C.; Davis, F. F. Alteration of immunological properties of bovine serum albumin by covalent attachment of polyethylene glycol. *J. Biol. Chem.* **1977**, *252* (11), 3578−81.
(53) Abuchowski, A.; McCoy, J. R.; Palczuk, N. C.; van Es, T.; Davis, F. F. Effect of covalent attachment of polyethylene glycol on immunogenicity and circulating life of bovine liver catalase. *J. Biol. Chem.* **1977**, *252* (11), 3582−6.
(54) Veronese, F. M.; Pasut, G. PEGylation, successful approach to drug delivery. *Drug Discovery Today* **2005**, *10* (21), 1451−8.
(55) Joralemon, M. J.; McRae, S.; Emrick, T. PEGylated polymers for medicine: from conjugation to self-assembled systems. *Chem. Commun. (Cambridge)* **2010**, *46* (9), 1377−93.
(56) Yamaoka, T.; Tabata, Y.; Ikada, Y. Distribution and tissue uptake of poly(ethylene glycol) with different molecular weights after intravenous administration to mice. *J. Pharm. Sci.* **1994**, *83* (4), 601−6.
(57) Kaminskas, L. M.; Boyd, B. J.; Karellas, P.; Krippner, G. Y.; Lessene, R.; Kelly, B.; Porter, C. J. The impact of molecular weight and PEG chain length on the systemic pharmacokinetics of PEGylated poly l-lysine dendrimers. *Mol. Pharmaceutics* **2008**, *5* (3), 449−63.
(58) Caliceti, P.; Veronese, F. M. Pharmacokinetic and biodistribution properties of poly(ethylene glycol)-protein conjugates. *Adv. Drug Delivery Rev.* **2003**, *55* (10), 1261−77.
(59) Knauf, M. J.; Bell, D. P.; Hirtzer, P.; Luo, Z. P.; Young, J. D.; Katre, N. V. Relationship of effective molecular size to systemic clearance in rats of recombinant interleukin-2 chemically modified with water-soluble polymers. *J. Biol. Chem.* **1988**, *263* (29), 15064−70.
(60) Seymour, L. W.; Miyamoto, Y.; Maeda, H.; Brereton, M.; Strohalm, J.; Ulbrich, K.; Duncan, R. Influence of molecular weight on passive tumour accumulation of a soluble macromolecular drug carrier. *Eur. J. Cancer* **1995**, *31A* (5), 766−70.
(61) Manjula, B. N.; Tsai, A.; Upadhya, R.; Perumalsamy, K.; Smith, P. K.; Malavalli, A.; Vandegriff, K.; Winslow, R. M.; Intaglietta, M.; Prabhakaran, M.; Friedman, J. M.; Acharya, A. S. Site-specific PEGylation of hemoglobin at Cys-93(beta): correlation between the colligative properties of the PEGylated protein and the length of the conjugated PEG chain. *Bioconjugate Chem.* **2003**, *14* (2), 464−72.